

A statistical model for droplet-wall interaction

Nicolás García Rosa, Philippe Villedieu, and Gérard Lavergne

ONERA/DMAE, 2, av. Edouard Belin, BP 4025, 31055 Toulouse Cedex 4, France

This paper presents a new model for the prediction of spray-wall impingement, based on a significant amount of experimental data, as well as on the review of several models previously proposed in the literature. This set of statistical correlations take into account the physical and dynamic properties of incident droplets, via the use of K number [1], which is a function of Ohnesorge and Weber numbers. For a broader application, dimensionless temperature number T^* [4], including boiling and Leidenfrost temperatures, is used to characterize the influence of wall temperature on interaction regimes. Explicit equations are given for the limits between interaction modes, the deposition rate and the size and velocity distributions of outgoing droplets, as a function of the above-cited dimensionless parameters. Comparisons with basic experiments from the literature lead to a partial validation. Validation on more complex configurations as well as the first applications on two-phase flow simulations of a real combustor are currently in progress and will be presented in a forthcoming paper.

I INTRODUCTION

The numerical simulation of complex two-phase flows in combustors with evaporating and impinging fuel sprays and wall films is a challenge for many years now. However, attempts to consider the interaction of gas flow, spray and wall film is only partial due to a lack of practicable models for spray/wall and spray/film interaction as well as wall-film propagation and evaporation.

Indeed, industrial codes, such as CEDRE [4] often use a Eulerian gas-flow solver coupled with a Lagrangian discrete-phase solver. The Lagrangian approach makes it extremely easy to implement statistical models for the complex phenomena encountered in two-phase flows. The major difficulty is obtaining reliable and validated models. For this purpose, basic experiments are conducted on simple configurations, such as isolated droplets or mono-sized droplet chains.

The literature concerning the general drop-wall impact problem is extremely wide (see [5] for a review) and an important number of numerical models have been derived, in the last 30 years, evidence of the extreme complexity of this phenomenon. Indeed, the studies on dry walls, thin sub-droplet size wall films ([14], [18] and [17]) and thick wall films, either hot or cold, all show a different behavior in terms of droplet impingement.

Based on the extensive experimental database acquired in the last two decades, and the numerous studies present in the literature, a reliable statistical spray/dry-wall interaction model is proposed hereafter. This new model aims at being the first general model covering a wide range of droplet physical and dynamic properties, as well as wall temperature.

Several limitations ought to be pointed out, though.

1. Only dry walls are considered. Indeed, the simulation of shear-driven wall films needs the development of a separate solver, which is out of the scope of this paper.
2. Only smooth walls are treated.
3. Transition interaction regimes are not modeled.
4. The case of icing walls will not be discussed here. By icing wall, we understand wall temperatures below the liquid fusion point. Icing is therefore out of the scope of the present model.

II PHENOMENOLOGY AND SCOPE

II.1 VISUALIZATION OF THE DIFFERENT INTERACTION REGIMES

The general layout of a basic experiment for the study of droplet impact on solid walls consists of a droplet generator injecting droplets against a solid wall. A high-speed video camera or a high-definition still camera (with appropriate triggering devices) is often used to observe the phenomena in detail. Droplet size and velocity can be measured by either digital image processing or phase-Doppler Particle Anemometry (P.D.P.A.) [6]. In the case of secondary atomization, laser diffraction can be used as well [7]. Droplet temperature can also be measured by means of Infra Red thermometry. An accurate characterization is then made of the impact outcome.

On a cold wall, i.e. for wall temperatures ranging between fusion and boiling points, heat transfer has a minor effect on the impact. Therefore, they can be disregarded, and two main kinds of interaction are observed: droplet deposition and droplet splashing.

When the velocity component normal to the wall is below a certain critical value, the droplet spreads on the wall, to reach a final position, after its initial kinetic energy has been partly dissipated by viscosity and partially transformed into surface tension.

For increasing impact velocities, viscous dissipation can no longer absorb the initial kinetic energy, and surface tension fails to maintain droplet cohesion. The droplet is then torn into smaller ones, some of which are ejected from the solid surface. The total ejected mass is usually inferior to the initial droplet mass. The amount of liquid that remains on the wall decreases as the collision velocity increases.

At high wall temperature, Leidenfrost effect is observed: the droplet surface in contact with the solid wall is immediately evaporated into a vapor cushion that isolates the drop from the solid surface. At low impingement velocity, this vapor cushion prevents the droplet from wetting the solid surface, therefore preserving its cohesion. Droplet rebound is then observed.

Table 2.1.1 presents the three main interaction regimes, as previously identified. Let us notice the fact that, at surface temperature higher than the liquid boiling

point, the intense heat transfer from the wall radically modifies the impact dynamics. Compare, for instance, figures 2.1.2 and 2.1.3. The first figure shows the formation of a cloud of very fine droplets. Cossali *et al* explain [6] that nucleate boiling at the solid surface creates vapor bubbles that explode at the free surface of the drop. These explosions originate the fine droplet cloud.

Intermediate regimes can also be observed, but in a much smaller range of impact velocities. These modes, often found near the limits between the three main ones, are particularly rare, and will not be included in the present model. An example is given in figure 2.1.1; notice the presence of two incident droplet sizes: the largest is torn into two while the small one simply bounces on the wall.

Figure 2.1.1 also points out a possible limitation to the use of droplet arrays for the study of isolated drops. Notice the small distance between two successive drops as they are squashed onto the solid surface. A higher injection frequency, or higher impact speed, would lead to coalescence on the wall. This should be thought as a subsidiary transition regime leading to film formation, which will not be discussed here. However, let us note that the case of droplet coalescence after impact, with no contact with the wall, is not necessarily in contradiction with the present model. The code in which the model is implemented should also host a coalescence model, as is the case for ONERA Lagrangian solver SPARTE [4].

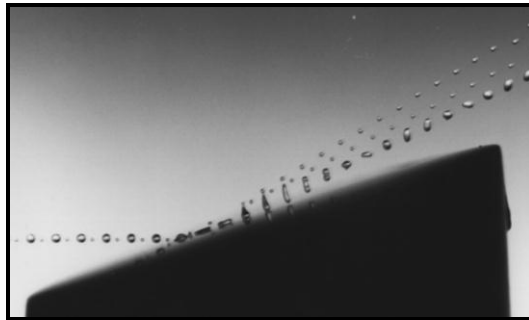


Fig. 0.1 – Example of a peculiar rebound mode, observed by [13], photo courtesy of *Album of Visualization*

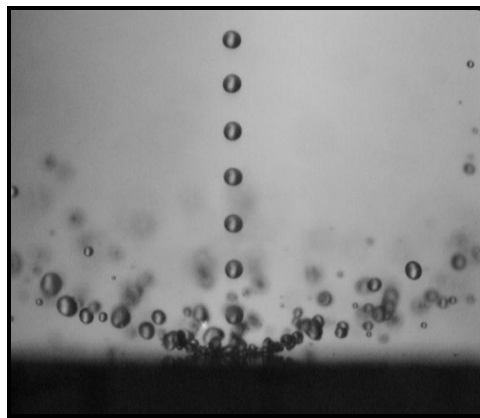




Fig. 0.2 – Splashing of an isooctane droplet stream on a very hot wall, $Oh = 9.93 \times 10^{-3}$, $We = 128$, $K = 814$, $T^* = 2.02$.

$We = 80$	$We = 7$
$K = 404$	$K = 45$
$T^* = 0.09$	$T^* = 1.58$
	
Droplet Deposition	Droplet Rebound

Tab. 0.1 – Main interaction regimes observed by [13] for ethyl-alcohol droplets, $Oh = 1.74 \times 10^{-2}$

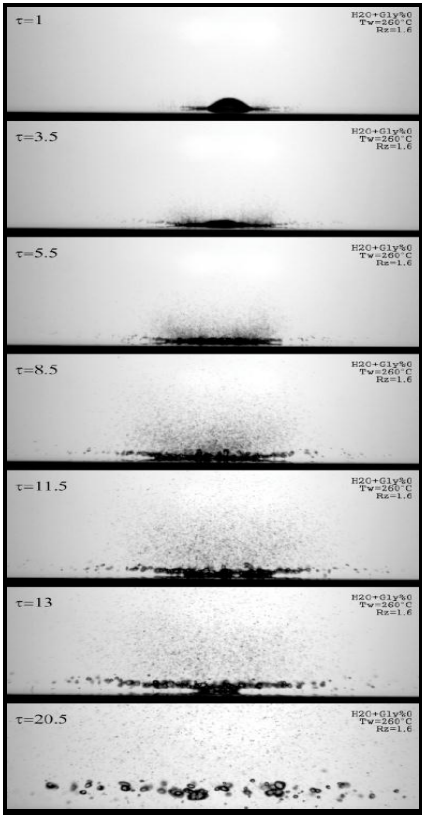


Fig. 0.3 – Droplet bubble-boiling splashing, observed in detail by [6] at 260°C wall temperature

II.2 DIMENSIONLESS PARAMETERS AND CLASSIFICATION OF THE DIFFERENT INTERACTION REGIMES

It is commonly observed that secondary atomization only takes place for impact velocity above a given critical value. Surface tension and impinging kinetic energy being critical to the outcome, Weber number is widely known to be representative of the impact regime.

$$We = \frac{\rho_\ell V^2 d}{\sigma_\ell} \quad (0.1)$$

Moreover, viscous dissipation plays an important part in the attenuation of surface instabilities, and is represented by a Reynolds number.

$$Re = \frac{\rho_\ell V d}{\mu_\ell} \quad (0.2)$$

Finally, the following dimensionless number, which is a function of the liquid boiling and Leidenfrost temperatures, represents the influence of wall temperature.

$$T^* = \frac{T_W - T_B}{T_L - T_B} \quad (0.3)$$

Boiling and Leidenfrost temperatures generally depend on the static air pressure. Therefore, T^* also represents the effects of air pressure.

The general problem, as described above, can then be described by those three dimensionless numbers, or any combination. Experimental studies also make use of the Ohnesorge number together with Weber number.

$$Oh = \frac{\sqrt{We}}{Re} = \frac{\mu_\ell}{\sqrt{\rho_\ell d \sigma_\ell}} \quad (0.4)$$

The limits between different regimes are commonly described in terms of a single dimensionless parameter. The following number, first proposed by Mundo *et al* [2] as a function of Weber and Reynolds numbers, depends on the droplet velocity via the Weber number only.

$$K = We \cdot Oh^{-\beta} \quad (0.5)$$

Several different values are found in the literature for the β parameter; however, Josserand and Zaleski [15] confirm the following value, via a purely theoretical approach. This value is also in agreement with the models presented by Mundo *et al* [2] and Marengo *et al* [3].

$$\beta = 2/5 = 0.4. \quad (0.6)$$

Experimental conditions are then represented, along with the observations, on a $K-T^*$ diagram, as in figure 2.2.1.

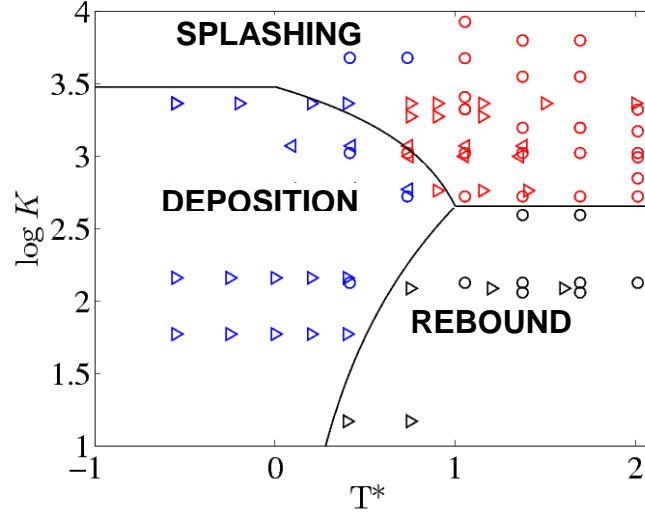


Fig. 0.2 – $\log K - T^*$ diagram. Experimental conditions from [5] (left-oriented triangles and circles) and [7] (right-oriented triangles) and observations : deposition (blue), splashing (red) and rebound (black) regimes

Denoting $T_1^* = 1$, equations $K_r(T^*)$ and $K_s(T^*)$ are defined for the limits and, for all $0 < T^* < T_1^*$, three interaction modes are then observed:

1. if $K < K_r(T^*)$ then the drop bounces on the solid surface and a small amount of its mass evaporates during contact,
2. if $K_r(T^*) < K < K_s(T^*)$ then the drop spreads on the wall and either evaporates completely or coalesces with the other drops on the wall, if any,
3. if $K_s(T^*) < K$ then the drop splashes and ejects a certain amount of its initial mass into a cloud of smaller droplets.

For wall temperatures above the liquid Leidenfrost temperature, $T_1^* < T^*$, Leidenfrost effect is observed, leading to only two different interaction modes:

4. if $K < K_r(T^*)$ then the droplet bounces and partially evaporates,
5. if $K_r(T^*) < K$ then the droplet splashes and partially evaporates.

Notice that, by definition, for all $T_1^* < T^*$, $K_r(T^*) = K_s(T^*)$.

By least squares fitting the experimental data of figure 2.2.1, the following expressions for the two limits are derived.

$$K_s(T^*) = \begin{cases} K_0 & T^* < 0 \\ K_0 + \frac{T^*}{T_1^*}(K_1 - K_0) & 0 < T^* < T_1^* \\ K_1 & T_1^* < T^* \end{cases} \quad (0.7)$$

where $T_1^* = 1$, $K_0 = 3000$ and $K_1 = 450$, and

$$K_r(T^*) = \begin{cases} 0 & T^* < 0 \\ K_1 \left[\frac{T^*}{T_1^*} \right]^\gamma & 0 < T^* < T_1^* \\ K_s(T^*) = K_1 & T_1^* < T^* \end{cases} \quad (0.8)$$

where $\gamma = 3$. Equations (2.2.7) and (2.2.8) determine the interaction regime, for a given set of impinging droplet characteristics. The next step in the modeling of such an impact is the prediction of the impact outcome, i.e. the outgoing droplet size and velocity distributions as well as the total ejected mass. The following sections present the equations for the modeling of droplet rebound and splashing.

III MODELING OF BOUNCE PHENOMENA

III.1 EVAPORATED MASS AND POST-IMPACT DROPLET DIAMETER

Droplet rebound is mainly encountered for wall temperatures above the liquid Leidenfrost temperature. Although most authors agree to assume the droplet mass to remain constant during the impact, the experimental study conducted by Le Clercq [11] shows a mass loss of up to 20%. Experiments were carried out with ethyl-alcohol droplets at ambient temperature. High-precision size measurements are done immediately after impact, using both Phase-Doppler Particle Analyzer (P.D.P.A.) and digital image processing. The main results are summarized in table 3.1.1. Let η_r be the ratio between the outgoing and the impinging liquid mass, the subscript r denoting the rebound regime,

$$\eta_r = \frac{m_a}{m_b}. \quad (0.1)$$

Despite the lack of experimental data, the following equation is proposed to take those results into account.

$$\eta_r = 1 - \chi \tanh \left[\left(\frac{Z}{Z_0} \right)^4 \right], \quad (0.2)$$

given the following definitions:

$$Z = K \cdot T^{*1/4}, \quad (0.3)$$

$$Z_0 = 145, \quad (0.4)$$

$$\chi = 0.25. \quad (0.5)$$

	Case	Case	Case	Case
d_b [μm]	250	220	210	210
$v_{b,n}$ [m/s]	0,93	1,03	1,18	1,26
α_b [$^\circ$]	15	15	14	15
T_w [K]	623	623	623	473
K [-]	101,7	107,1	132,9	151,5
T^* [-]	2,48	2,48	2,48	1,11
d_a [μm]	239	205	192	193
η_r [-]	0,87	0,81	0,76	0,78

Tab. 0.1 – Sample experimental data by Le Clercq [11] of droplet rebound on a hot wall

Equation (3.1.2) also takes into account the fact that the evaporation rate increases with impact velocity, and therefore, with K number. A maximum evaporation of 25% of the initial mass is arbitrarily set to avoid erroneous extrapolation of the available data. Post-impact droplet diameter is then derived from equation (3.1.1):

$$d_a = \eta_r^{1/3} \cdot d_b. \quad (0.6)$$

III.2 POST-IMPACT DROPLET VELOCITY

In order to take into account the influence of wall temperature, the model proposed by Béard [10] is extended into the following dimensionless form,

$$\frac{We_{n,a}}{We_1(T^*)} = 16 \times \left[\sqrt{\frac{K_b}{K_r(T^*)}} - \frac{K_b}{K_r(T^*)} \right]^2, \quad (0.1)$$

where $We_{n,a}$ denotes the Weber number based on the normal component of the reflected droplet velocity, and

$$We_1(T^*) = 3.5 \times \frac{T^{*2}}{1 + T^{*2}}. \quad (0.2)$$

Figures 3.2.1 and 3.2.2 plot the normal velocity after impact as a function of the normal velocity before impact, for a wide range of droplet size and wall temperature number T^* . The plot shapes agree with the Wachters and Westerling model [1]. As can be expected, for an increasing solid surface temperature, the outgoing droplet velocity increases as well, as the Leidenfrost effect grows. On the other hand, for a given droplet diameter, there exists an impinging velocity for which the post-rebound velocity is zero. This value is clearly a function of T^* , and corresponds to the critical Weber number above which the interaction regime is no longer rebound but droplet splashing.

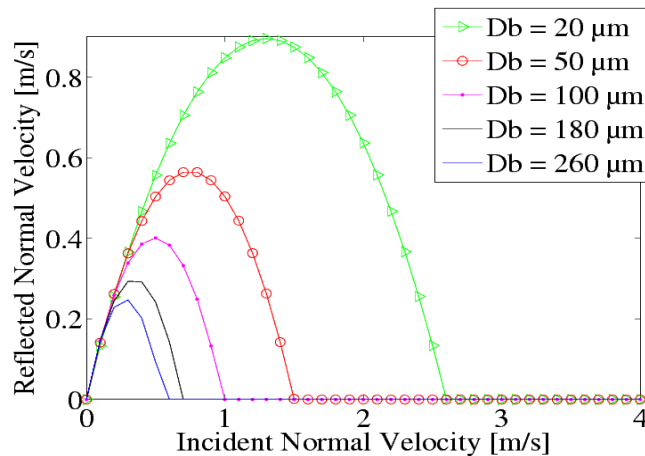


Fig. 0.1 – Normal component of velocity for reflected droplet as a function of normal component of impinging velocity and droplet size, ethyl-alcohol drops, $T_w = 400$ K ($0 < T^* < 1$)

Regarding the velocity component tangent to the wall, constant velocity damp is assumed during impact [11], which leads to

$$\vec{V}_{t,a} = e \cdot \vec{V}_{t,b} \quad (0.3)$$

where $e = 0.8$.

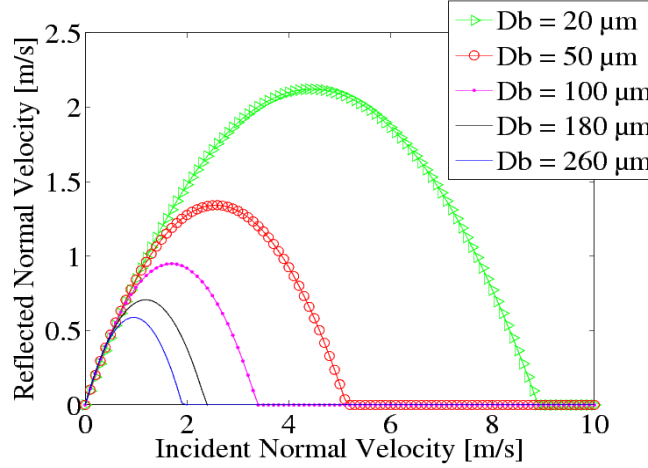


Fig. 0.2 – Normal component of velocity for reflected droplet as a function of normal component of impinging velocity and droplet size, ethyl-alcohol drops, $T_w = 700$ K ($T^* \approx 3$)

III.3 POST-IMPACT DROPLET TEMPERATURE

To our knowledge, the work of Le Clercq [11], [12] is the only attempt to measure droplet temperature. By means of an infrared device, surface temperature is measured immediately after impact. It was observed that surface temperature returned to its initial value immediately after impact, even for wall temperatures 200 K hotter than the droplet. Indeed, Leidenfrost effect tends to isolate the droplet from the wall and contact time is extremely short. Moreover, evaporation compensates part of the heating. Therefore, droplet temperature can be assumed to remain constant.

IV MODELING OF SPLASHING PHENOMENA

IV.1 EVAPORATED MASS

In spite of its importance for practical applications, only a few correlations for the mass ratio η_s can be found in the literature. However, for a cold solid surface ($T^* < 0$), mass loss can only be due to a partial deposition on the wall, therefore, η_s should be a function of K only. For wall temperatures between boiling and Leidenfrost points, mass loss is due to both partial deposition and evaporation, and η_s should be a function of both K and T^* . Finally, for higher temperatures, $T^* > 1$, no deposition is observed and there is a strong similarity with the case of droplet rebound, for which a correlation has been derived in the previous section.

In anticipation of future experimental data, the following equation, plotted in figure 4.1.1 is proposed,

$$\eta_s(T^*) = \eta_0(T^*) \left[1 - \left[\frac{K_s(T^*)}{K} \right]^{\beta_0(T^*)} \right] + \eta_1(T^*) \quad (0.1)$$

with K_s defined in section 2 and η_0 , η_1 and β_0 defined here after,

$$\eta_0(T^*) = \begin{cases} 0.75 & T^* < 0 \\ 0.75 \times (1 - T^*) & 0 < T^* < T_1^* \\ 0 & T_1^* < T^* \end{cases} \quad (0.2)$$

$$\eta_1(T^*) = \begin{cases} 0 & T^* < 0 \\ 0.75 \times T^* & 0 < T^* < T_1^* \\ 0.75 & T_1^* < T^* \end{cases} \quad (0.3)$$

$$\beta_0(T^*) = \begin{cases} 1 & T^* < 0 \\ 1 - T^* & 0 < T^* < T_1^* \\ 0 & T_1^* < T^* \end{cases} \quad (0.4)$$

The maximum mass ratio is set to 0.75, which agrees with both the model presented by Bai and Gossman [16] and the evaporation rate measured by Le Clercq [11], [12]. The fact of having the terms η_0 and β_0 be a function of T^* leads to a continuous evolution from cold wall ($T^* < 0$) to hot wall ($T^* > 1$).

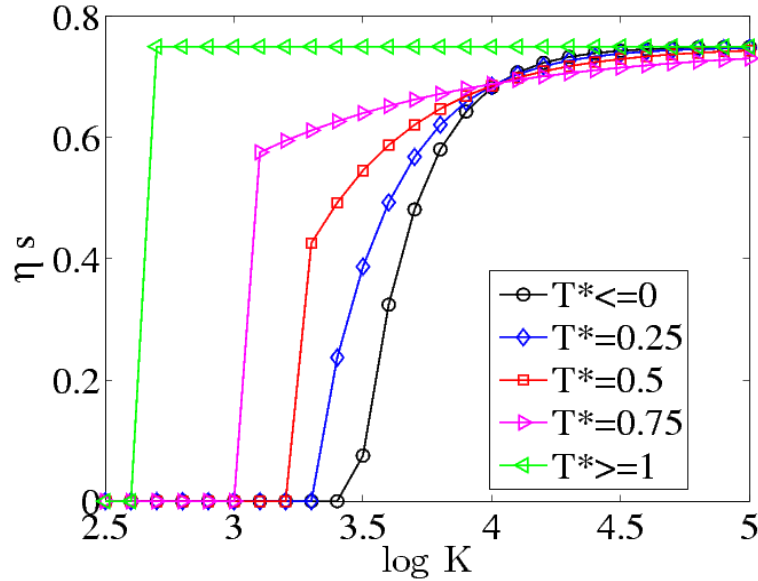


Fig. 0.1 – Droplet mass ratio η_s after splashing impact, as a function of K and T^* numbers.

IV.2 POST-IMPACT DROPLET VELOCITY

The model that will be introduced in this section is inspired from the model derived by Schmell *et al* [17] and the works of Mundo *et al* [2]. In this approach, impinging droplet velocity is decomposed into two components, one perpendicular to the solid wall, and the other, parallel to the solid surface, respectively denoted

$\bar{v}_{n,b}$ and $\bar{v}_{t,b}$. The phenomenon is then separated into two kinds of contributions: normal splashing and tangential splashing. Tangential splashing only originates a nonzero tangential splashed velocity $\bar{v}'_{t,a}$ whereas normal splashing originates a splashed velocity \bar{v}''_a , which is neither normal nor tangential. The final splashed velocity is obtained by adding the two contributions, giving $\bar{v}_a = \bar{v}'_{t,a} + \bar{v}''_a$.

After a normal splashing, the following Weibull probability law determines the magnitude of vector \bar{v}''_a ,

$$P(x) = \frac{b}{\theta} \left[\frac{x}{\theta} \right]^{b-1} \exp \left[- \left[\frac{x}{\theta} \right]^b \right], \quad (0.1)$$

where $b = 2.5$, $\theta = 0.35$ and

$$x = \frac{\|\bar{v}''_a\|}{\|\bar{v}_{n,b}\|}. \quad (0.2)$$

Then, the orientation of vector \bar{v}''_a is defined by its elevation α and azimuth β , which are determined using a uniform probability law, in the ranges of 0° to 25° for α and 0° to 360° for β . Having angle β take any possible value from an arbitrarily-set reference axis, agrees with the fact that a normal impact originates a symmetrical cloud of splashed drops.

Tangential splashing will be regarded as a constant tangent velocity damp, which leads to

$$\bar{v}'_{t,a} = e \cdot \bar{v}_{t,b}, \quad (0.3)$$

where $e = 0.8$

IV.3 POST-IMPACT DROPLET SIZE

The splashing impact of a single droplet creates a cloud of smaller droplets with a lognormal size distribution of the form given below,

$$P(d) = \frac{1}{\sqrt{2\pi} \cdot \sigma_d} \exp \left[- \frac{1}{2\sigma^2} \left(\ln \frac{d}{d_m} \right)^2 \right]. \quad (0.1)$$

It is defined by the two following parameters, mean diameter d_m and variance σ . Experimental data often use the Sauter mean diameter (SMD) after impact, which can then be calculated by the following expression,

$$d_m = d_{32,a} \cdot \exp \left[-5 \frac{\sigma^2}{2} \right]. \quad (0.2)$$

Fitting of experimental data from [7] and [17] leads to the following correlation,

$$\frac{d_{32,a}}{d_b} = R_0 + R_1 \exp \frac{-K}{\Delta K_0} \quad (0.3)$$

where $R_0 = 0.15$, $R_1 = 0.85$ and $\Delta K_0 = 1500$. Let us notice that this model does not take into account the influence of wall temperature, which has been observed to be

relatively weak, as shown in figure 4.3.1. Regarding distribution variance, although a simple correlation could not be derived, the following constant is proposed, as found in several experimental histograms from [7].

$$\sigma = 0.45 \quad (0.4)$$

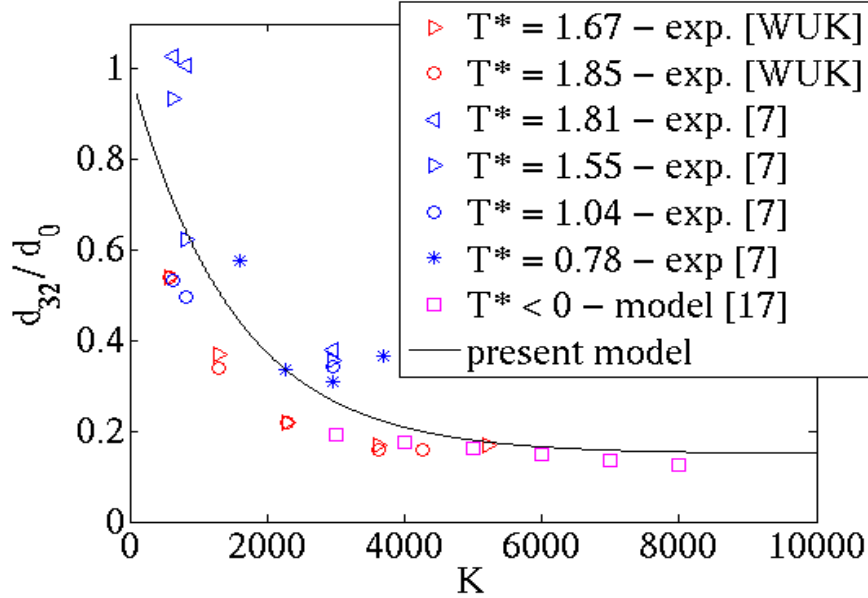


Fig. 0.1 – Post-impact SMD to initial droplet size ratio, as a function of K number and wall temperature number T^* , exp. denotes experimental data.

IV.4 POST-IMPACT DROPLET TEMPERATURE

To our knowledge, no reliable experimental data, from which a model could be derived, currently exist in the literature. In anticipation of such results, let us assume the splashed secondary droplets temperature to be that of the impinging droplet. This assumption comes to completely neglecting heat transfer from the solid wall during splashing impact.

V VALIDATION

In anticipation of future experimental studies, partial validation of droplet size probability density function (PDF) prediction for splashing impacts is presented in this section. The results of the present model are compared to P.D.P.A. measurements by Richter [8]. Note that these results were not used to establish the model and were saved for validation purposes.

In the frame of the EGISTHE French research program supported by the French military agency (DGA), the present model has been implemented in the Lagrangian solver of ONERA CEDRE code. Some comparisons have been carried out between numerical results and experimental data concerning the impact of a mono-sized droplet chain impinging a hot wall. The three pictures bellow show a good qualitative agreement on the direction of the outgoing droplets for both the splashing and the bouncing regimes.

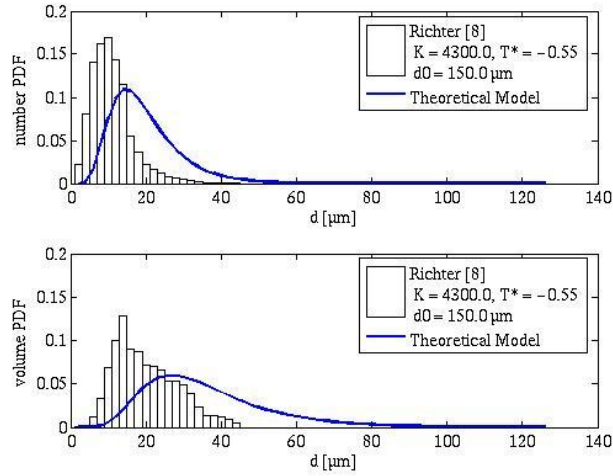


Fig. 5.1 – Number and Volume Probability Density Functions of droplet size after splashing impact ($K = 4300$). Experimental measurements [8] vs. theoretical model.

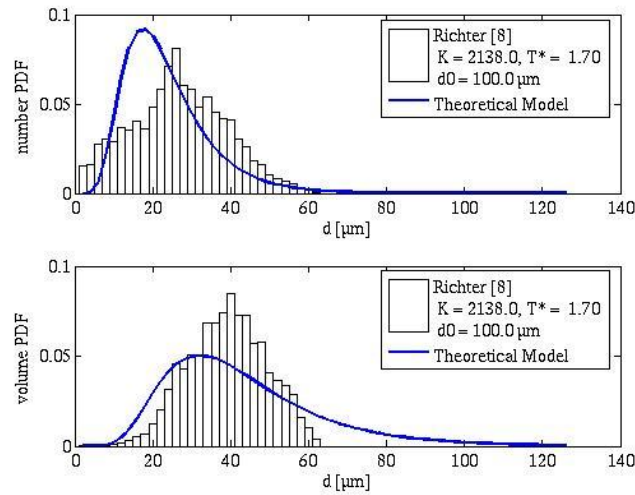


Fig. 5.2 – Number and Volume Probability Density Functions of droplet size after splashing impact ($\log K = 3.33$). Experimental measurements [8] vs. theoretical model.

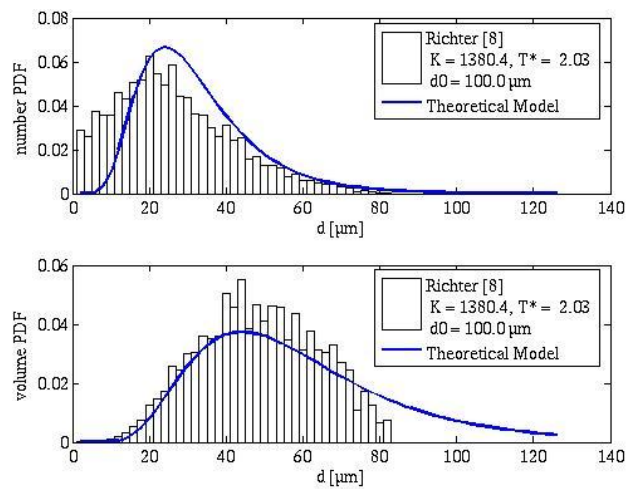


Fig. 5.3 – Number and Volume Probability Density Functions of droplet size after splashing impact ($\log K = 3.62$). Experimental measurements [8] vs. theoretical model.

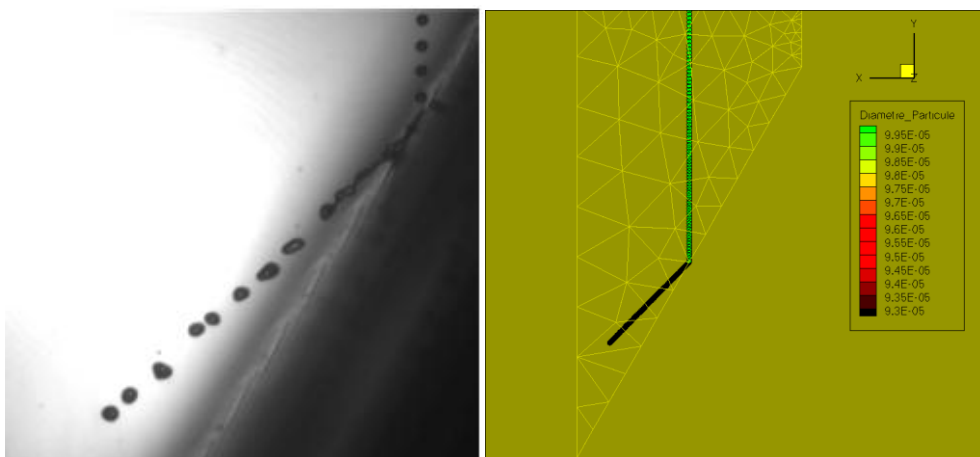


Fig. 5.4 - Bouncing of iso-octane droplets on a hot wall (up : CEDRE result, down : experimental result). $T^* = 1.44$, $K=382$, impact angle : 30° .

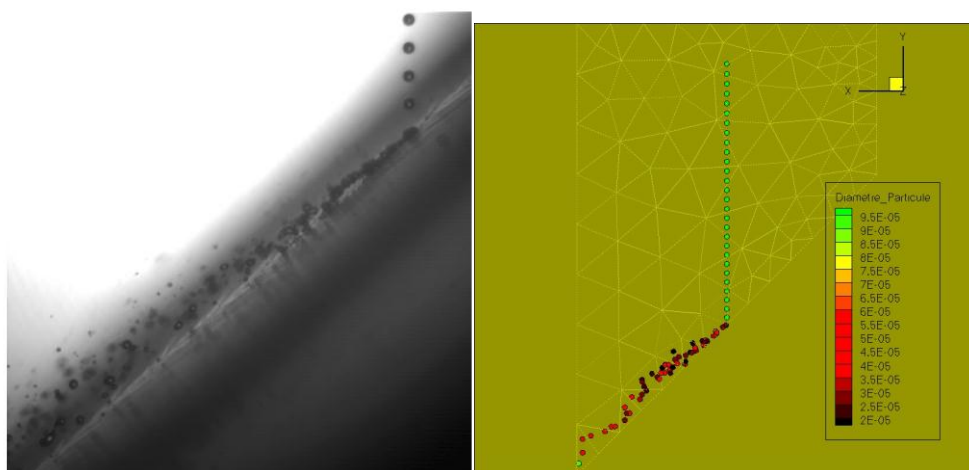


Fig. 5.5 - Splashing of iso-octane droplets on a hot wall (up : CEDRE result, down : experimental result). $T^* = 1.96$, $K=1020$, impact angle : 45° .

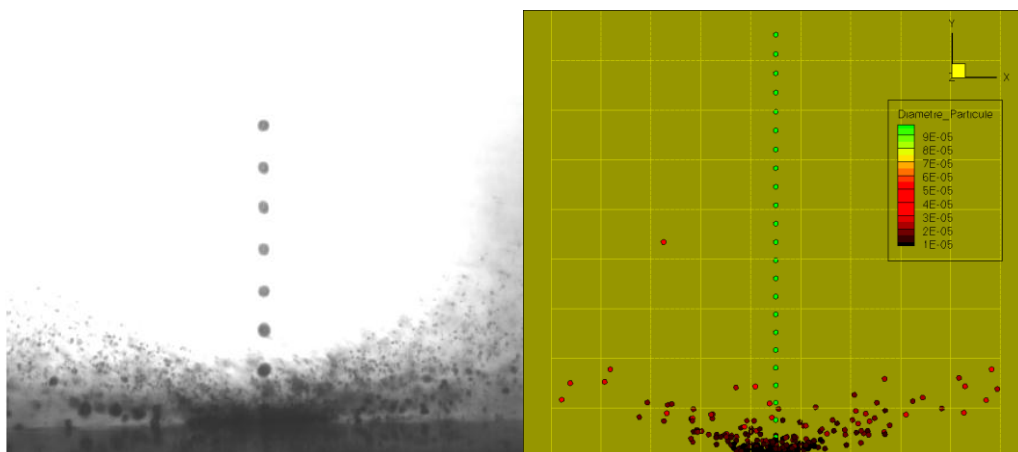


Fig. 5.6 - Splashing of iso-octane droplets on a hot wall (up : CEDRE result, down : experimental result). $T^* = 1.96$, $K= 4591$, impact angle : 90° .

VI CONCLUSION

Although figures 4.4.1 to 4.4.6 show a satisfactory agreement for a wide range of wall temperature, this validation is only partial. Indeed, a statistical model as the one presented in this paper ought to be validated on complex configurations, such as polydisperse spray impact on walls. Such work is currently under progress and will determine the extent to which this model is accurate and robust.

VII NOMENCLATURE

Symbols			Subscripts	
d	[μm]	Particle diameter	l	Liquid
d_{32}	[μm]	Sauter Mean Diameter (SMD)	b	Before: pre-impact conditions
m	[KG]	Droplet mass	a	After: post-impact conditions
$P(d)$	[-]	Droplet size PDF	s	Splashing
$P(v)$	[-]	Droplet velocity PDF	r	Rebound
T_w	[K]	Wall temperature	d	Deposition
T_B	[K]	Boiling point temperature	n	Normal component of vector
T_L	[K]	Leidenfrost Temperature	t	Tangential component of vector
T	[K]	Droplet temperature		
v	[m/s]	Droplet normal velocity		
α	[°]	Angle of incidence from surface normal		
η	[-]	Mass ratio		
μ	[Pl]	Dynamic viscosity		
ρ	[kg/m ³]	Density		
σ	[-]	Variance		
σ_ℓ	[N/m]	Liquid surface tension		

VIII REFERENCES

1. L.M.J. Wachters, & N.A.J. Westerling, The heat transfer from a hot wall to impinging water drops in the spheroidal state, Chemical Eng. Sciences, vol. 21, pp. 1047-1056, 1966.
2. C.H.R. Mundo, M. Sommerfeld, & C. Tropea, Droplet-wall collisions: experimental studies of the deformation and break-up process, Int. J. of Multiphase Flow, vol. 21, No. 2, pp.151-173, 1995.
3. M. Marengo, S. Sikalo, and C. Tropea, Impact of drops on inclined dry surfaces, Proc. ILASS Europe, Manchester (United Kingdom), 1998.

4. Chevalier P., Courbet B., Dutoya D., Klotz P., Ruiz E., Troyes J., Villedieu P., CEDRE: development and validation of a multiphysic computational software. 1st European Conference for Aerospace Sciences (EUCASS), Moscow, Russia, 2005
5. G.E. Cossali, M. Marengo and M. Santini, Single-drop empirical models for spray impact on solid walls: a review, *Atomization and Sprays*, vol. 15, pp. 699-736, 2005
6. G.E. Cossali, M. Marengo and M. Santini, Secondary atomisation produced by single drop vertical impacts onto heated surfaces, *Experimental Thermal and Fluid Science*, Volume 29, Issue 8, September 2005, Pages 937-946
7. J. Dewitte, P. Berthoumieu, G. Lavergne, An Experimental Study of Droplet Hot Wall Interactions and a Survey of the Splashing Regime, 5th International Symposium on Multiphase Flow, Heat Mass Transfer and Energy Conversion, ISMF 05 Xi'an, China, 3-6 July 2005
8. B. Richter, K. Dullenkopf, and H.J. Bauer, Investigation of secondary droplet characteristics produced during wall impact, 12th Int. Symp. On the Application of Laser Techniques to Fluid Mechanics, Lisbon, 2004.
9. Ph. Béard, Y. Biscos, G. Lavergne, A. Rompteaux, Experimental and numerical studies of turbulent dispersion in two-phase flows, 5th Int. Symp. On Refined Flow Modelling – Paris, September 1993
10. Ph. Béard, Modélisation lagrangienne de la dispersion et de l'évaporation de gouttes dans un écoulement turbulent instationnaire, Ph.D. thesis, École Nationale Supérieure de l'Aéronautique et de l'Espace, 1994.
11. C. Amiel, P. le Clercq, O. Ravel, G. Lavergne, P. Berthoumieu, J. Farré, Use of an infrared detector to analyze the temperature evolution of a droplet impacting on a heating wall, 15th Annual Int. Symp. On Aerospace Defence Sensing and Controls (AEROSENSE) – Orlando, USA, 16—20 April 2001.
12. P. Le Clercq, Contribution à l'étude expérimentale et théorique des interactions gouttes/paroi, Ph.D. thesis, École Nationale Supérieure de l'Aéronautique et de l'Espace, 2000.
13. C. Amiel, Application de techniques optiques à l'étude du comportement dynamique et thermique de gouttes en interaction avec une paroi chauffée, Ph.D. thesis, École Nationale Supérieure de l'Aéronautique et de l'Espace, 2002.
14. S. Giroud-Garapon, Étude du comportement d'un film liquide dans les chambres de combustion de statoréacteurs et/ou turboréacteurs, Ph.D. thesis, École Nationale Supérieure de l'Aéronautique et de l'Espace, 2003.
15. C. Josserand and S. Zaleski, Droplet splashing on a thin liquid film, *Phys. of Fluids*, vol. 15, No. 6, pp. 1650-1657, 2003.
16. C. Bai, and A.D. Gosman, Development of methodology for spray impingement situation, SAE Paper 950283, 1995.
17. R. Schmehl, H. Roskamp, M. Willmann, S. Wittig, CFD Analysis of Spray Propagation and Evaporation Including Wall Film Formation and Spray/Film Interactions, *Int. J. of Heat and Fluid Flow*, Vol. 20, n° 5, pp. 520-529, 1999.
18. W. Samenfink, A. Elsässer, K. Dullenkopf, & S. Wittig, Droplet interaction with shear-driven liquid films: analysis of deposition and secondary droplet characteristics, *Int. J. of Heat and Fluid Flow*, vol. 20, pp. 462-469, 1999.

Summary of derived correlations

$K_s(T^*) = \begin{cases} K_0 & T^* < 0 \\ K_0 + \frac{T^*}{T_1^*} (K_1 - K_0) & 0 < T^* < T_1^* \\ K_1 & T_1^* < T^* \end{cases} \quad \begin{matrix} T_1^* = 1 \\ K_0 = 3000 \\ K_1 = 450 \\ \gamma = 3 \end{matrix}$			$K_r(T^*) = \begin{cases} 0 & T^* < 0 \\ K_l \left[\frac{T^*}{T_1^*} \right]^\gamma & 0 < T^* < T_1^* \\ K_s(T^*) = K_l & T_1^* < T^* \end{cases}$																		
Droplet Deposition	Droplet Splashing	Droplet Rebound																			
$K_r(T^*) < K < K_s(T^*)$ $T^* < T_1^*$		$K_s(T^*) < K$		$K < K_r(T^*)$																	
$\eta_s(T^*) = \eta_0(T^*) \left[1 - \left[\frac{K_s(T^*)}{K} \right]^{\beta_0(T^*)} \right] + \eta_l(T^*)$																					
$\eta_d = 0$			$\eta_r = 1 - \chi \tanh \left[\left(\frac{Z}{Z_0} \right)^4 \right]$																		
			$Z = K \cdot T^{*1/4}$																		
			$Z_0 = 145$																		
			$\chi = 0.25$																		
<table><tr><th></th><th>$T^* < 0$</th><th>$0 < T^* < T_1^*$</th><th>$T_1^* < T^*$</th></tr><tr><td>$\eta_0(T^*) =$</td><td>0.75</td><td>$0.75 \times (1 - T^*)$</td><td>0</td></tr><tr><td>$\eta_l(T^*) =$</td><td>0</td><td>$0.75 \times T^*$</td><td>0.75</td></tr><tr><td>$\beta_0(T^*) =$</td><td>1</td><td>$1 - T^*$</td><td>0</td></tr></table>				$T^* < 0$	$0 < T^* < T_1^*$	$T_1^* < T^*$	$\eta_0(T^*) =$	0.75	$0.75 \times (1 - T^*)$	0	$\eta_l(T^*) =$	0	$0.75 \times T^*$	0.75	$\beta_0(T^*) =$	1	$1 - T^*$	0			
	$T^* < 0$	$0 < T^* < T_1^*$	$T_1^* < T^*$																		
$\eta_0(T^*) =$	0.75	$0.75 \times (1 - T^*)$	0																		
$\eta_l(T^*) =$	0	$0.75 \times T^*$	0.75																		
$\beta_0(T^*) =$	1	$1 - T^*$	0																		
$P(d) = \frac{1}{\sqrt{2\pi} \cdot \sigma d} \exp \left[-\frac{1}{2\sigma^2} \left(\ln \frac{d}{d_m} \right)^2 \right]$																					
$P(d) = 0$			$\sigma = 0.45$																		
			$d_m = d_{32,a} \cdot \exp \left[-5 \frac{\sigma^2}{2} \right]$																		
			$\frac{d_{32,a}}{d_b} = R_0 + R_1 \exp \frac{-K}{\Delta K_0}$																		
			$R_0 = 0.15 \quad R_1 = 0.85 \quad \Delta K_0 = 1500$																		
$\vec{v}_a = \vec{v}'_{t,a} + \vec{v}''_a$																					
$P(v) = 0$			$x = \frac{\ \vec{v}''_a\ }{\ \vec{v}_{n,b}\ }; \quad P(x) = \frac{b}{\theta} \left[\frac{x}{\theta} \right]^b \exp \left[-\left[\frac{x}{\theta} \right]^b \right]$																		
			$b = 2.5$																		
			$\theta = 0.35$																		
			$\alpha \text{ in } [0^\circ, 25^\circ] \text{ (see section 0)}$ $\beta \text{ in } [0^\circ, 360^\circ] \text{ (see section 0)}$																		
$\vec{v}'_{t,a} = e \cdot \vec{v}_{t,b}, \quad e = 0.8$			$\frac{We_{n,a}}{We_l(T^*)} = 16 \times \left[\sqrt{\frac{K_b}{K_r(T^*)}} - \frac{K_b}{K_r(T^*)} \right]^2$ $We_l(T^*) = 3.5 \times \frac{T^{*2}}{1 + T^{*2}}$																		
			$\vec{v}_{t,a} = e \cdot \vec{v}_{t,b}, \quad e = 0.8$																		
$T_a = T_b$	$T_a = T_b$	$T_a = T_b$																			

